

**CCC Publications**



# Adaptive Backstepping Sliding Mode Fault-Tolerant Control of Quadrotor UAV in the presence of external disturbances, uncertainties, and Simultaneous Actuator and Sensor faults

A. Ezzara\*, A.Y. Ouardine, H. Ayad

**Abderrahim Ezzara\***

LSEEET Laboratory, Department of Applied Physics  
Faculty of Science and Technology, Cadi Ayyad University, Marrakesh, Morocco  
\*Corresponding author: abderrahim.ezzara@ced.uca.ma

**Ahmed Youssef Ouardine**

Ecole Royale de l'Air, Marrakesh, Morocco  
a.y.ouadine@gmail.com

**Hassan Ayad**

LSEEET Laboratory, Department of Applied Physics  
Faculty of Science and Technology, Cadi Ayyad University, Marrakesh, Morocco  
h.ayad@uca.ma

## Abstract

This paper presents a new active fault-tolerant control strategy for quadrotor unmanned aerial vehicles against simultaneous unknown external disturbances, system uncertainties, actuator faults, and sensor faults, which pose critical safety risks in autonomous flight operations. Unlike existing approaches that handle these challenges separately, the proposed method provides an integrated solution for simultaneous actuator and sensor fault compensation. Based on a quadrotor's nonlinear dynamic model, time-varying actuator and sensor faults are simultaneously estimated by a nonlinear unknown input observer, and to attenuate the effect of disturbances on fault estimation, an  $\mathcal{H}_\infty$  performance index is used. Subsequently, a robust nonlinear adaptive backstepping sliding mode control technique is proposed to actively compensate for the estimated faults while maintaining stability despite the presence of uncertainties and disturbances. Simulation results in MATLAB demonstrate successful fault estimation convergence and robust control performance across various challenging scenarios with different fault combinations and operational conditions. The proposed strategy achieves high tracking accuracy with attitude RMSE below  $10^{-3}$  rad with position RMSE below 0.2 m under concurrent actuator and sensor fault conditions.

**Keywords:** Active fault-tolerant control, quadrotor UAV, actuator and sensor faults, nonlinear unknown input observer, adaptive backstepping sliding mode control.

## 1 Introduction

In recent years, quadrotors as unmanned aerial vehicles (UAVs) have become increasingly vital in various fields. However, their widespread use also raises significant security concerns, including potential system failures and external disturbances. Ensuring quadrotors' reliability and resilience in the face of such challenges is critical for their effective operation in both civilian and military applications.

To address these challenges, fault-tolerant control (FTC) systems have become a focal point of research. Recent research has focused extensively on developing FTC strategies for quadrotors to address uncertainties, disturbances, actuator, and sensor faults. In [1], [2], [3], and [4] authors address actuator faults and/or disturbances and uncertainties for quadrotor; however, it lacks coverage of sensor faults and uncertainties. In [5], authors study the diagnosis and compensation for sensors and actuator constant faults in a quadrotor UAV in the presence of uncertainties and external disturbances using a feedback linearization technique and a nonlinear high-gain observer, excluding time-varying faults. A new FTC strategy for quadrotors under time-varying sensor faults and disturbances based on a disturbance observer and a non-singular fast terminal sliding mode algorithm is proposed in [6], excluding actuator faults and uncertainties. Finally, [7] introduces a robust backstepping control strategy that includes an adaptive observer for actuator faults, missing sensor faults, disturbances, and uncertainties. Other FTC strategies are proposed in [8], [9], [10].

Existing FTC approaches for quadrotor UAVs often ignore full fault coverage, especially regarding time-varying faults. Unlike previous strategies [1]-[10], neither has examined the handling of both time-varying sensor and actuator faults in the presence of uncertainties and external disturbances.

For fault estimation (FE), in [11], the authors suggest a novel nonlinear unknown input observer (NUIO), but they didn't take into consideration the effect of system uncertainties. In [12], [13], and [14], the proposed NUO with partly decoupled disturbances must meet a rank condition, which limits its use to many real systems. In [15], authors didn't consider sensor faults. Inspired by [16], a novel NUO with disturbance attenuation without rank requirement for the quadrotor model is proposed. This NUO is integrated with backstepping and sliding mode control (SMC) techniques to handle time-varying external disturbances, uncertainties, actuator and sensor faults.

The main contributions of this paper are: (1) The use of a complete nonlinear model of the quadrotor UAV taking into consideration different nonlinearities; (2) The development of a novel NUO to simultaneously estimate actuator and sensor faults without any rank requirement in the system model, even in the presence of uncertainties and external disturbances. (3) Solving the observer design problem using  $\mathcal{H}_\infty$  optimization through a linear matrix inequality (LMI) formulation. (4) Design and implementation of an adaptive backstepping sliding mode FTC controller utilizing the NUO-based fault estimation. (5) Addressing parametric uncertainties, wind disturbances, noise, and different types of time-varying additive and multiplicative actuator and sensor faults.

The remainder of this study is organized as follows: Section II provides a description of the quadrotor nonlinear dynamic model. Various actuator and sensor fault types are modeled in this section. In Section III, using the  $\mathcal{H}_\infty$  optimization, a NUO is constructed to simultaneously estimate the actuator and the sensor faults. Section IV provides a robust adaptive backstepping SMC (ABSMC) strategy to handle system failure effects. Finally, Section V shows a validation of the proposed FTC using MATLAB simulations.

## 2 Quadrotor Nonlinear Dynamical modeling

### 2.1 Quadrotor dynamical modeling

The quadrotor dynamical model can be derived using the Newton-Euler formalism. Let's introduce two reference frames, let E (O, X, Y, Z) designate an inertial frame, and B (o, x, y, z) designate a frame permanently coupled to the quadrotor body as illustrated in Figure 1. Both of them are assumed to be at the center of gravity of the quadrotor UAV.

The absolute position of the quadrotor may be obtained by the three coordinates ( $x, y, z$ ) and its attitude by the three Euler angles, respectively roll  $\phi$ , pitch  $\theta$ , and yaw  $\psi$ .

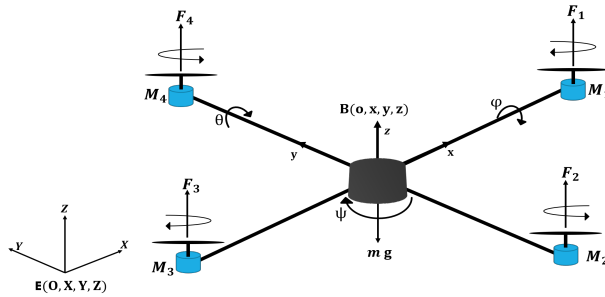


Figure 1: Quadrotor configuration

The quadrotor's dynamic model, which considers the drag forces, aerodynamic friction torques, and torques due to the gyroscopic effects, is given as in [17] by:

$$\ddot{\phi} = \frac{1}{I_x} (\dot{\theta}\dot{\psi}(I_y - I_z) - K_{fax}\dot{\phi}^2 - J_r\bar{\Omega}\dot{\theta} + dU_2) \quad (1a)$$

$$\ddot{\theta} = \frac{1}{I_y} (\dot{\phi}\dot{\psi}(I_z - I_x) - K_{fay}\dot{\theta}^2 + J_r\bar{\Omega}\dot{\phi} + dU_3) \quad (1b)$$

$$\ddot{\psi} = \frac{1}{I_z} (\dot{\theta}\dot{\phi}(I_x - I_y) - K_{faz}\dot{\psi}^2 + U_4) \quad (1c)$$

$$\ddot{x} = \frac{1}{m} ((C\phi S\theta C\psi + S\phi S\psi)U_1 - K_{ftx}\dot{x}) \quad (1d)$$

$$\ddot{y} = \frac{1}{m} ((C\phi S\theta S\psi - S\phi C\psi)U_1 - K_{fty}\dot{y}) \quad (1e)$$

$$\ddot{z} = \frac{1}{m} (C\phi C\theta U_1 - K_{ftz}\dot{z}) - g \quad (1f)$$

where  $C$  is the trigonometrical function cosine, and  $S$  is the function sine,  $m$  is the total mass of the quadrotor,  $g$  is the gravity acceleration constant,  $I_x$ ,  $I_y$ , and  $I_z$  are the constants inertia,  $K_{ftx}$ ,  $K_{fty}$ , and  $K_{ftz}$  are the translation drag coefficients,  $K_{fax}$ ,  $K_{fay}$ , and  $K_{faz}$  are the coefficients of aerodynamic friction around  $X$ ,  $Y$ , and  $Z$ .  $d$  is the distance between the center of mass of the quadrotor and the rotation axis of the propellers,  $J_r$  is the rotor inertia,  $\bar{\Omega}$  represents the disturbance caused by the rotor unbalance,  $U_1$ ,  $U_2$ ,  $U_3$ , and  $U_4$  represent the quadrotor control inputs.

Based on the angular speeds of the four rotors, the control inputs and the disturbance  $\bar{\Omega}$  are expressed as follows:

$$\begin{bmatrix} U_1 \\ U_2 \\ U_3 \\ U_4 \end{bmatrix} = \begin{bmatrix} K_p & K_p & K_p & K_p \\ -K_p & 0 & K_p & 0 \\ 0 & -K_p & 0 & K_p \\ K_d & -K_d & K_d & -K_d \end{bmatrix} \begin{bmatrix} \omega_1^2 \\ \omega_2^2 \\ \omega_3^2 \\ \omega_4^2 \end{bmatrix} \quad (2)$$

$$\bar{\Omega} = \omega_1 - \omega_2 + \omega_3 - \omega_4 \quad (3)$$

where  $K_p$  is the lift coefficient,  $K_d$  is the drag coefficient, and  $\omega_i$  for  $i \in \{1, 2, 3, 4\}$  are the angular rotor speeds.

The control inputs remain restricted by the motors' maximum rotational speeds  $\omega_{\max}$ , which are illustrative of their physical constraints:

$$\begin{aligned} 0 &\leq U_1 \leq 4K_p\omega_{\max}^2 \\ -K_p\omega_{\max}^2 &\leq U_2 \leq K_p\omega_{\max}^2 \\ -K_p\omega_{\max}^2 &\leq U_3 \leq K_p\omega_{\max}^2 \\ -2K_d\omega_{\max}^2 &\leq U_4 \leq 2K_d\omega_{\max}^2 \end{aligned} \quad (4)$$

From equations (1d) to (1f), the expressions of the nonholonomic constraints can be extracted:

$$\tan \theta = \frac{(\ddot{x} + \frac{K_{ftx}}{m} \dot{x})C_\psi + (\ddot{y} + \frac{K_{fty}}{m} \dot{y})S_\psi}{\ddot{z} + g + \frac{K_{ftz}}{m} \dot{z}} \quad (5a)$$

$$\sin \phi = \frac{(\ddot{x} + \frac{K_{ftx}}{m} \dot{x})S_\psi - (\ddot{y} + \frac{K_{fty}}{m} \dot{y})C_\psi}{\sqrt{(\ddot{x} + \frac{K_{ftx}}{m} \dot{x})^2 + (\ddot{y} + \frac{K_{fty}}{m} \dot{y})^2 + (\ddot{z} + g + \frac{K_{ftz}}{m} \dot{z})^2}} \quad (5b)$$

Nonholonomic constraints will be used to produce the desired pitch ( $\theta_d$ ) and roll ( $\phi_d$ ).

## 2.2 Disturbances, uncertainties, and faults modeling

To simulate the effect of wind disturbances, the Von Karman model will be used in this paper [18, 19, 20]. Wind disturbances will be noted  $d_0(t)$  in the rest of this paper and given by:

$$d_0 = [d_\phi, d_\theta, d_\psi, d_x, d_y, d_z]^T \quad (6)$$

where  $d_\phi$ ,  $d_\theta$ , and  $d_\psi$  represents the disturbance affecting the quadrotor's attitude. And  $d_x$ ,  $d_y$ , and  $d_z$  are the disturbances along the X, Y and Z axes, respectively.

Additional parameter uncertainties in the quadrotor model are considered for the translation drag coefficients  $K_{ftx}$ ,  $K_{fty}$ , and  $K_{ftz}$ , and the aerodynamic friction coefficients  $K_{fax}$ ,  $K_{fay}$ , and  $K_{faz}$ . Based on the system model given by (1), the uncertainties effect can be expressed as follows:

$$\begin{aligned} \xi_\phi &= -\frac{\Delta K_{fax}}{I_x} \dot{\phi}^2, & \xi_\theta &= -\frac{\Delta K_{fay}}{I_y} \dot{\theta}^2, & \xi_\psi &= -\frac{\Delta K_{faz}}{I_z} \dot{\psi}^2, \\ \xi_x &= -\frac{\Delta K_{ftx}}{m} \dot{x}, & \xi_y &= -\frac{\Delta K_{fty}}{m} \dot{y}, & \xi_z &= -\frac{\Delta K_{ftz}}{m} \dot{z} \end{aligned} \quad (7)$$

where  $\Delta K_{fax}$ ,  $\Delta K_{fay}$ ,  $\Delta K_{faz}$ ,  $\Delta K_{ftx}$ ,  $\Delta K_{fty}$ , and  $\Delta K_{ftz}$  represent the uncertainties of  $K_{fax}$ ,  $K_{fay}$ ,  $K_{faz}$ ,  $K_{ftx}$ ,  $K_{fty}$ , and  $K_{ftz}$  respectively. The uncertainty vector will be noted  $\xi(x, t)$  and given by  $\xi = [\xi_\phi, \xi_\theta, \xi_\psi, \xi_x, \xi_y, \xi_z]^T$ .

Common actuator faults include Bias fault, Loss of Effectiveness fault, and Actuator Stuck fault [21, 22]. The combined equation for these faults can be described using:

$$f_a(t) = -\epsilon u(t) + f_{a0}(t) \quad (8)$$

where  $f_a$  is the actuator fault,  $u$  denotes the system control input,  $\epsilon \in [0, 1]$  denotes the actuator gain variation coefficient, and  $f_{a0}$  is an actuator fault function, and  $f_a = [f_{a1}, f_{a2}, f_{a3}, f_{a4}]^T$ .

Common sensor faults include bias fault, drift fault, loss of effectiveness fault, and stuck sensor fault [23, 24]. The combined equation for these faults can be described using:

$$f_s(t) = -\rho y(t) + f_{s0}(t) \quad (9)$$

where  $f_s$  is the sensor fault,  $y$  denotes system output,  $\rho \in [0, 1]$  denotes the sensor gain variation coefficient, and  $f_{s0}$  is a sensor fault function, and  $f_s = [f_{s1}, f_{s2}, f_{s3}, f_{s4}, f_{s5}, f_{s6}]^T$ .

## 2.3 Complete nonlinear quadrotor dynamic model

Let's define the system's state vector given by:

$$x = [x_1, \dots, x_{12}]^T = [\phi, \dot{\phi}, \theta, \dot{\theta}, \psi, \dot{\psi}, x, \dot{x}, y, \dot{y}, z, \dot{z}]^T \quad (10)$$

The system output vector is given by:

$$y = [x_1, x_2 - f_{s1}, x_3, x_4 - f_{s2}, x_5, x_6 - f_{s3}, x_7, x_8 - f_{s4}, x_9, x_{10} - f_{s5}, x_{11}, x_{12} - f_{s6}]^T \quad (11)$$

From equations (1) and considering uncertainties, disturbances, actuators, and sensor faults modeled above, the following state-space model is obtained:

$$\begin{aligned}
 \dot{x}_1 &= x_2 \\
 \dot{x}_2 &= a_1 x_4 x_6 + a_2 x_2^2 + a_3 \bar{\Omega} x_4 + b_1 U_2 + f_{a1} + d_\phi + \xi_\phi \\
 \dot{x}_3 &= x_4 \\
 \dot{x}_4 &= a_4 x_2 x_6 + a_5 x_4^2 + a_6 \bar{\Omega} x_2 + b_2 U_3 + f_{a2} + d_\theta + \xi_\theta \\
 \dot{x}_5 &= x_6 \\
 \dot{x}_6 &= a_7 x_2 x_4 + a_8 x_6^2 + b_3 U_4 + f_{a3} + d_\psi + \xi_\psi \\
 \dot{x}_7 &= x_8 \\
 \dot{x}_8 &= a_9 x_8 + U_x \frac{U_1}{m} + d_x + \xi_x \\
 \dot{x}_9 &= x_{10} \\
 \dot{x}_{10} &= a_{10} x_{10} + U_y \frac{U_1}{m} + d_y + \xi_y \\
 \dot{x}_{11} &= x_{12} \\
 \dot{x}_{12} &= a_{11} x_{12} - g + \frac{\cos(x_1) \cos(x_3)}{m} U_1 + f_{a4} + d_z + \xi_z
 \end{aligned} \tag{12}$$

where

$$\begin{aligned}
 a_1 &= \frac{I_y - I_z}{I_x}, & a_2 &= -\frac{K_{fax}}{I_x}, & a_3 &= -\frac{J_r}{I_x}, & a_4 &= \frac{I_z - I_x}{I_y}, & a_5 &= -\frac{K_{fay}}{I_y} \\
 a_6 &= \frac{J_r}{I_y}, & a_7 &= \frac{I_x - I_y}{I_z}, & a_8 &= -\frac{K_{faz}}{I_z}, & a_9 &= -\frac{K_{ftx}}{m}, & a_{10} &= -\frac{K_{fty}}{m} \\
 a_{11} &= -\frac{K_{ftz}}{m}, & b_1 &= \frac{d}{I_x}, & b_2 &= \frac{d}{I_y}, & b_3 &= \frac{1}{I_z}.
 \end{aligned}$$

### 3 NUIO-based FE design

The following state-space form can be employed to represent the complete model (12):

$$\begin{aligned}
 \dot{x}(t) &= Ax(t) + Bu(t) + \Phi(x, t) + F_a f_a(t) + Dd(t) \\
 y(t) &= Cx(t) + F_s f_s(t)
 \end{aligned} \tag{13}$$

where  $x \in \mathbb{R}^{12}$  and given by (10),  $y \in \mathbb{R}^{12}$  and given by (11), the control input vector is given by  $u = [U_1, U_2, U_3, U_4]^T$ .  $F_a \in \mathbb{R}^{12 \times 4}$  and  $F_s \in \mathbb{R}^{12 \times 6}$  are known constant distribution matrices.  $d \in \mathbb{R}^6$  represent lumped uncertainty that includes both external disturbances and system uncertainties.  $\Phi \in \mathbb{R}^{12}$  is a continuous known nonlinear function vector.  $A \in \mathbb{R}^{12 \times 12}$ ,  $B \in \mathbb{R}^{12 \times 4}$ ,  $C \in \mathbb{R}^{12 \times 12}$ , and  $D \in \mathbb{R}^{12 \times 6}$  are known constant matrices.

For the development of the considered observer, the following conditions must be satisfied [16]:

*Assumption 1:* The pair  $(A, C)$  is observable, the pair  $(A, B)$  is controllable, and  $\text{rank}(B, F_a) = \text{rank}(B)$ .

*Assumption 2:* The unknown input disturbances  $d$  is bounded with unknown upper bounds such that  $d \in L_2[0, \infty)$ .

*Assumption 3:* The faults  $f_a$  and  $f_s$  belong to  $L_2[0, \infty)$ , and  $f_a$  and  $f_s$  are continuously smooth with bounded first-time derivatives.

*Assumption 4:*  $\Phi(x, t)$  satisfies the Lipschitz property with respect to  $x$ , such that:

$$\|\Phi(x, t) - \Phi(\hat{x}, t)\| \leq L_f \|x - \hat{x}\| \quad \forall x, \hat{x} \in \mathbb{R}^{12} \tag{14}$$

where  $L_f$  is a positive constant.

For our system, assumptions 1 to 4 are satisfied, and as a consequence, the developement of the cited observer is feasible.

The following augmented system state space is obtained by considering actuator and sensor faults as auxiliary states.

$$\begin{aligned}\dot{\bar{x}} &= \bar{A}\bar{x} + \bar{\Phi}(A_0\bar{x}, t) + \bar{B}u + \bar{D}\bar{d} \\ y &= \bar{C}\bar{x}\end{aligned}\quad (15)$$

where

$$\begin{aligned}\bar{x} &= \begin{bmatrix} x \\ f_a \\ f_s \end{bmatrix}, \quad \bar{A} = \begin{bmatrix} A & F_a & 0 \\ 0 & 0 & 0 \\ 0 & 0 & 0 \end{bmatrix}, \quad \bar{B} = \begin{bmatrix} B \\ 0 \\ 0 \end{bmatrix}, \quad \bar{D} = \begin{bmatrix} D & 0 & 0 \\ 0 & I_4 & 0 \\ 0 & 0 & I_6 \end{bmatrix} \\ \bar{C} &= [C \ 0 \ F_s], \quad \bar{\Phi}(A_0\bar{x}, t) = \begin{bmatrix} \Phi(x, t) \\ 0 \end{bmatrix}, \quad \bar{d} = \begin{bmatrix} d \\ \dot{f}_a \\ \dot{f}_s \end{bmatrix}, \quad A_0 = [I_{12} \ 0 \ 0]\end{aligned}$$

A NUIO estimates the augmented state  $\bar{x}$  as follows:

$$\begin{aligned}\dot{z} &= Mz + Gu + N\bar{\Phi}(A_0\hat{\bar{x}}, t) + Ly \\ \hat{\bar{x}} &= z + Hy\end{aligned}\quad (16)$$

where  $z \in \mathbb{R}^{22}$  is the observer system state and  $\hat{\bar{x}} \in \mathbb{R}^{22}$  is the estimate of  $\bar{x}$ . The matrices  $M \in \mathbb{R}^{22 \times 22}$ ,  $G \in \mathbb{R}^{22 \times 4}$ ,  $N \in \mathbb{R}^{22 \times 22}$ ,  $L \in \mathbb{R}^{22 \times 12}$ , and  $H \in \mathbb{R}^{22 \times 12}$  are to be designed.

The estimation error is stated as  $e = \bar{x} - \hat{\bar{x}}$ , it's time derivative is given by:

$$\begin{aligned}\dot{e} &= (T\bar{A} - L_1\bar{C})e + (T\bar{A} - L_1\bar{C} - M)z + (T\bar{B} - G)u \\ &\quad + [(T\bar{A} - L_1\bar{C})H - L_2]y + T\bar{\Phi}(\bar{A}_0x, t) - N\bar{\Phi}(\bar{A}_0\hat{x}, t) + T\bar{D}\bar{d}\end{aligned}\quad (17)$$

where  $T = I_{22} - H\bar{C}$  and  $L = L_1 + L_2$ . The observer matrices  $M$ ,  $G$ ,  $N$ , and  $L_2$  are given by:

$$M = T\bar{A} - L_1\bar{C}, \quad N = T, \quad G = T\bar{B}, \quad L_2 = (T\bar{A} - L_1\bar{C})H \quad (18)$$

Substituting (18) into (17), and assuming the effect of system nonlinearity on the FE observer is negligible, since this simplification allows for a more tractable analysis without significant loss of accuracy, the error dynamics become:

$$\begin{aligned}\dot{e} &= (T\bar{A} - L_1\bar{C})e + T\bar{D}\bar{d} \\ z_e &= C_e e\end{aligned}\quad (19)$$

where  $z_e$  is the measured output used to verify the observer performance and  $C_e \in \mathbb{R}^{22 \times 22}$ .

In contrast to studies [11]-[15], this work addresses the attenuation of disturbance, without any rank requirement in the system model, using resilient design, rather than complete decoupling.

A sufficient requirement for the existence of a NUIO (16), is given by Theorem 1 below:

**Theorem 1.** *Given a positive scalar  $\gamma$ , the system error (19) is asymptotically stable with  $\mathcal{H}_\infty$  performance  $\|G_{z_e\bar{d}}\|_\infty < \gamma$ , if there exists a symmetric positive definite matrix  $P \in \mathbb{R}^{22 \times 22}$ , and matrices  $M_1 \in \mathbb{R}^{22 \times 12}$  and  $M_2 \in \mathbb{R}^{22 \times 12}$  such that*

$$\begin{bmatrix} \Omega_1 & \Omega_2 \\ \Omega_2^T & -\gamma^2 I_{16} \end{bmatrix} < 0 \quad (20)$$

where  $\Omega_1 = He[P\bar{A} - M_1\bar{C}\bar{A} - M_2\bar{C}] + C_e^T C_e$  and  $\Omega_2 = (P - M_1\bar{C})\bar{D}$ . And  $He(V) = V + V^\top$  for a given matrix  $V$ .

*Proof.* Lets consider the following Lyapunov function

$$V_e = e^T P e \quad (21)$$

where  $e$  is by (19) and  $P$  is a symmetric positive definite matrix, then

$$\begin{aligned}\dot{V}_e &= \dot{e}^T P e + e^T P \dot{e} \\ &= e^T H e [P(T\bar{A} - L_1\bar{C})]e + H e [e^T P T \bar{D} \bar{d}]\end{aligned}\quad (22)$$

The  $\mathcal{H}_\infty$  performance  $\|G_{z_e \bar{d}}\|_\infty < \gamma$  is given by

$$J = \int_0^\infty (z_e^T z_e - \gamma^2 \bar{d}^T \bar{d}) dt < 0 \quad (23)$$

Under zero initial conditions, (23) becomes

$$\begin{aligned}J &= \int_0^\infty (z_e^T z_e - \gamma^2 \bar{d}^T \bar{d} + \dot{V}_e) dt - \int_0^\infty \dot{V}_e dt \\ &= \int_0^\infty (z_e^T z_e - \gamma^2 \bar{d}^T \bar{d} + \dot{V}_e) dt - (V_e(\infty) - V_e(0)) \\ &\leq \int_0^\infty (z_e^T z_e - \gamma^2 \bar{d}^T \bar{d} + \dot{V}_e) dt\end{aligned}\quad (24)$$

To satisfy (23), the following sufficient condition is required

$$J_1 = z_e^T z_e - \gamma^2 \bar{d}^T \bar{d} + \dot{V}_e < 0 \quad (25)$$

Substituting (22) into (25) yields

$$J_1 = z_e^T z_e - \gamma^2 \bar{d}^T \bar{d} + e^T H e [P(T\bar{A} - L_1\bar{C})]e + H e [e^T P T \bar{D} \bar{d}] < 0 \quad (26)$$

By defining  $M_1 = PH$  and  $M_2 = PL_1$ , the condition (26) is satisfied if

$$\begin{bmatrix} \Omega_1 & \Omega_2 \\ \Omega_2^T & -\gamma^2 I_{16} \end{bmatrix} < 0 \quad (27)$$

where  $\Omega_1 = He[P\bar{A} - M_1\bar{C}\bar{A} - M_2\bar{C}] + C_e^T C_e$  and  $\Omega_2 = (P - M_1\bar{C})\bar{D}$ .  $\square$

The matrices  $P$ ,  $M_1$ ,  $M_2$ , and  $L_1$  are obtained by solving the Linear Matrix Inequality (LMI) given in equation (27). The LMIs were solved using CVX, a MATLAB-based modeling system for convex optimization. From these, the matrices  $H$  and  $L_1$  are computed as:

$$H = P^{-1}M_1, \quad L_1 = P^{-1}M_2 \quad (28)$$

Matrices  $H$  and  $L_1$  are then used to derive the matrices  $T$ ,  $M$ ,  $N$ ,  $G$ , and  $L$  through the equations provided in equation (18).

## 4 Backstepping Sliding Mode Fault-Tolerant Controller Design

The proposed control approach is based on two loops, the internal loop has four control laws ( $U_1$ ,  $U_2$ ,  $U_3$ , and  $U_4$ ), and the external loop has two virtual control laws ( $U_x$  and  $U_y$ ). The synoptic scheme (Figure 2) below illustrates this control strategy.

The synthesized stabilizing control laws are as described in the following:

$$U_2 = \frac{1}{b_1} [\ddot{\phi}_d - a_1 x_4 x_6 - a_2 x_2^2 - a_3 \bar{\Omega} x_4 - k_1 \dot{e}_1 - A_1 \dot{s}_1 - s_1 - A_2 s_2 - \hat{f}_{a1} - \dot{\hat{f}}_{s1} - \hat{\Gamma}_1 \text{sign}(s_2)] \quad (29a)$$

$$U_3 = \frac{1}{b_2} [\ddot{\theta}_d - a_4 x_7 x_9 - a_5 x_8^2 - a_6 \bar{\Omega} x_7 - k_3 \dot{e}_3 - A_3 \dot{s}_3 - s_3 - A_4 s_4 - \hat{f}_{a2} - \dot{\hat{f}}_{s2} - \hat{\Gamma}_2 \text{sign}(s_4)] \quad (29b)$$

$$U_4 = \frac{1}{b_3} [\ddot{\psi}_d - a_7 x_7 x_8 - a_8 x_9^2 - k_5 \dot{e}_5 - A_5 \dot{s}_5 - s_5 - A_6 s_6 - \hat{f}_{a3} - \dot{\hat{f}}_{s3} - \hat{\Gamma}_3 \text{sign}(s_6)] \quad (29c)$$

$$U_x = \frac{m}{U_1} [\ddot{x}_d - a_9 x_{10} - k_7 \dot{e}_7 - A_7 \dot{s}_7 - s_7 - A_8 s_8 - \dot{\hat{f}}_{s4} - \hat{\Gamma}_4 \text{sign}(s_8)] \quad (29d)$$

$$U_y = \frac{m}{U_1} [\ddot{y}_d - a_{10} x_{11} - k_9 \dot{e}_9 - A_9 \dot{s}_9 - s_9 - A_{10} s_{10} - \dot{\hat{f}}_{s5} - \hat{\Gamma}_5 \text{sign}(s_{10})] \quad (29e)$$

$$U_1 = \frac{m}{c x_1 c x_2} [\ddot{z}_d - a_{11} x_{12} + g - k_{11} \dot{e}_{11} - A_{11} \dot{s}_{11} - s_{11} - A_{12} s_{12} - \hat{f}_{a4} - \dot{\hat{f}}_{s6} - \hat{\Gamma}_6 \text{sign}(s_{12})] \quad (29f)$$

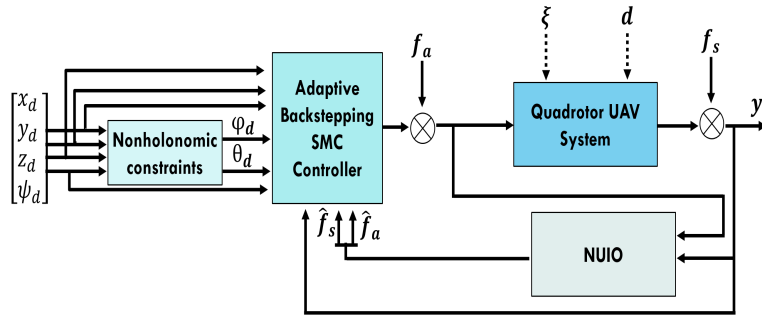


Figure 2: Synoptic scheme illustrating the control strategy.

*Proof.* Lets demonstrate the expression of  $U_2$ , considering the following roll subsystem:

$$\begin{cases} \dot{x}_1 = x_2 \\ \dot{x}_2 = \Phi_1 + b_1 U_2 + f_{a1} + d_\phi + \xi_\phi \end{cases} \quad (30)$$

where  $\Phi_1 = a_1 x_4 x_6 + a_2 x_2^2 + a_3 \bar{\Omega} x_4$ .

The output subsystem vector is given by  $[y_1 \ y_2 - f_{s1}] = [x_1 \ x_2 - f_{s1}]$ , where  $f_{s1}$  is a sensor fault.

**Step 1:** Define the control error as  $e_1 = y_1 - y_{1d} = x_1 - x_{1d}$ . The sliding surface equation is:

$$s_1 = e_1 + k_1 \int e_1 dt \quad k_1 > 0 \quad (31)$$

The Lyapunov function chosen is:

$$V_1 = \frac{1}{2} s_1^2 \quad (32)$$

The time derivative of  $V_1$  is:

$$\begin{aligned} \dot{V}_1 &= s_1 \dot{s}_1 = s_1 (\dot{e}_1 + k_1 e_1) \\ &= s_1 (y_2 + f_{s1} - \dot{x}_{1d} + k_1 e_1) \end{aligned} \quad (33)$$

The virtual control input is chosen as  $(y_2)_d = \alpha_1 = \dot{x}_{1d} - k_1 e_1 - A_1 s_1 - \hat{f}_{s1} - \alpha_{s1}$ . Where  $\alpha_{s1}$  is a nonlinear damping remains to be determined.

Substituting the virtual control value of  $(y_2)_d$ ,  $\dot{V}_1$  becomes:

$$\dot{V}_1 = -A_1 s_1^2 - s_1 (\alpha_{s1} - \tilde{f}_{s1}) \quad (34)$$

where  $\tilde{f}_{s1} = f_{s1} - \hat{f}_{s1}$ . Choosing  $\alpha_{s1} = k_{s1} \text{sign}(s_1)$ , where  $\text{sign}(\cdot)$  denotes the sign function and  $k_{s1} > 0$ .

Equation (34) becomes:

$$\begin{aligned} \dot{V}_1 &= -A_1 s_1^2 - s_1 (k_{s1} \text{sign}(s_1) - \tilde{f}_{s1}) \\ &\leq -A_1 s_1^2 - |s_1| (k_{s1} - |\tilde{f}_{s1}|) \end{aligned} \quad (35)$$

Suppose there exists a positive constant  $k_{s1}$ , such that  $|\tilde{f}_{s1}| \leq k_{s1}$ .

Finally, the equation (35) becomes

$$\dot{V}_1 \leq -A_1 s_1^2 \leq 0 \quad (36)$$

**Step 2:** The second sliding surface is:

$$s_2 = y_2 - \alpha_1 = y_2 - \dot{x}_{1d} + k_1 e_1 + A_1 s_1 + \hat{f}_{s1} + \alpha_{s1} \quad (37)$$

The derivative of  $s_2$  over time is:

$$\dot{s}_2 = \Phi_1 + b_1 U_2 + f_{a1} + d_\phi + \xi_\phi - \dot{f}_{s1} - \ddot{x}_{1d} + k_1 \dot{e}_1 + A_1 \dot{s}_1 + \dot{\hat{f}}_{s1} + \dot{\alpha}_{s1} \quad (38)$$

Based on the principle of certain equivalence,  $f_{a1}$  and  $d_\phi$  are replaced by their estimates. Using the sliding surface in equation (38), the input control  $U_2$  is given by:

$$U_2 = \frac{1}{b_1} \left[ \ddot{\phi}_d - \Phi_1 - k_1 \dot{e}_1 - A_1 \dot{s}_1 - s_1 - A_2 s_2 - \hat{f}_{a1} - \dot{\hat{f}}_{s1} - \hat{\Gamma}_1 \text{sign}(s_2) \right] \quad (39)$$

where  $\dot{\hat{\Gamma}}_1 = \beta_1 |s_2|$ , and  $\beta_1$  is a positive constant. Replacing  $U_2$  in equation (39),  $\dot{s}_2$  becomes

$$\dot{s}_2 = \tilde{f}_{a1} + d_\phi + \xi_\phi - \dot{f}_{s1} - \dot{\alpha}_{s1} - s_1 - \hat{\Gamma}_1 \text{sign}(s_2) - A_2 s_2 \quad (40)$$

The presence of the terms  $\tilde{f}_{a1}$ ,  $d_\phi$ ,  $\xi_\phi$ ,  $\dot{f}_{s1}$ , and  $\dot{\alpha}_{s1}$  in the expression of  $\dot{s}_2$  does not assert the system stability. To overcome this obstacle, the Lyapunov function is increased by adding a square term involving  $\tilde{\Gamma}_1$ .

$$V_2 = \frac{1}{2} (s_1^2 + s_2^2) + \frac{1}{2\beta_1} \tilde{\Gamma}_1^2 \quad (41)$$

where  $\tilde{\Gamma}_1 = \Gamma_1 - \hat{\Gamma}_1$ , and  $\hat{\Gamma}_1$  is the estimate of  $\Gamma_1$  (assuming  $\dot{\Gamma}_1 \approx 0$ ). Its derivative is

$$\begin{aligned} \dot{V}_2 &= s_1 \dot{s}_1 + s_2 \dot{s}_2 + \frac{1}{\beta_1} \tilde{\Gamma}_1 \dot{\tilde{\Gamma}}_1 \\ &= s_1 (s_2 - A_1 s_1) + s_2 \dot{s}_2 - (\Gamma_1 - \hat{\Gamma}_1) |s_2| \\ &\leq -A_1 s_1^2 - A_2 s_2^2 + \hat{\Gamma}_1 (|s_2| - s_2 \text{sign}(s_2)) + |s_2| (|\tilde{f}_{a1} + d_1 + \xi_1 - \dot{f}_{s1} - \dot{\alpha}_{s1} - \Gamma_1|) \\ &\leq -A_1 s_1^2 - A_2 s_2^2 + |s_2| (|\tilde{f}_{a1} + d_\phi + \xi_\phi - \dot{f}_{s1} - \dot{\alpha}_{s1}| - \Gamma_1) \end{aligned} \quad (42)$$

*Assumption 5:* There exists an unknown parameter  $\Gamma_1 > 0$ , such that:

$$|\tilde{f}_{a1} + d_\phi + \xi_\phi + \dot{f}_{s1} - \dot{\alpha}_{s1}| \leq \Gamma_1 \quad (43)$$

Thus,  $\dot{V}_2 \leq 0$  if  $|\tilde{f}_{a1} + d_\phi + \xi_\phi + \dot{f}_{s1} - \dot{\alpha}_{s1}| \leq \Gamma_1$ .

The same steps are followed to extract  $U_3$ ,  $U_4$ ,  $U_x$ ,  $U_y$  and  $U_z$ .

To avoid non-differentiability and chattering phenomena, the sign function will be replaced by a smooth function.

$$\text{sign}(s, \delta) = \frac{s}{\|s\| + \delta} \quad (44)$$

where  $\delta$  is a small positive constant.  $\square$

## 5 Simulation Results and Analysis

To evaluate the performance of the proposed FTC, simulations were executed in the MATLAB-SIMULINK® environment across three conditions. Condition 1 involved trajectory tracking with wind disturbances and model uncertainties. Condition 2 introduced actuator faults alongside these disturbances and uncertainties. Condition 3 further expanded to include both actuator and sensor faults in addition to wind disturbances and uncertainties.

The quadrotor subject of our study is the Draganfly IV manufactured by Draganfly Innovations. Parameter identification is studied in [25] and summarized below:

Table 1: Quadrotor Model Parameters

Parameter	Value
$m$	400 g
$g$	9.81 m/s <sup>2</sup>
$d$	20.5 cm
$K_P$	$2.9842 \times 10^{-5}$ N/rad/s
$J_r$	$2.8385 \times 10^{-5}$ N.m/rad/s <sup>2</sup>
$K_d$	$3.232 \times 10^{-7}$ N.m/rad/s
$I_x, I_y, I_z$	$(3.8278, 3.8278, 7.1345) \times 10^{-3}$ N.m/rad/s <sup>2</sup>
$K_{ftx}, K_{fty}, K_{ftz}$	$(3.2, 3.2, 4.8) \times 10^{-2}$ N/m/s
$K_{fax}, K_{fay}, K_{faz}$	$(5.567, 5.567, 6.354) \times 10^{-4}$ N/rad/s

For the Observer design purpose, choosing  $C_e = I_{22}$ ,  $\gamma = 0.5$ , and  $L_f = 35$ .

### Condition 1: Trajectory tracking with only wind disturbances and uncertainties

In Simulink, the "Von Karman Wind Turbulence Model" block was used to produce time-varying wind gusts as output. In our model, the mean wind speeds are of 5 m/s for attitude and 8 m/s for position. The figure 3 illustrates the varying velocity of wind disturbances over time.

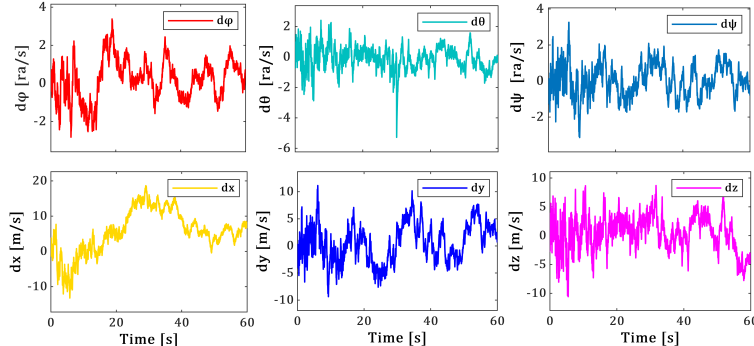


Figure 3: Wind disturbances velocity profile using Von Kármán model.

It is assumed that  $K_{ftx}$ ,  $K_{fty}$ , and  $K_{ftz}$ , as well as  $K_{fax}$ ,  $K_{fay}$ , and  $K_{faz}$ , are subject to a parametric uncertainty of 15% ( $\Delta K_{ftx} = 0.15K_{ftx}$ ).

Figure 4 display excellent tracking accuracy and stability despite wind disturbances and uncertainties, showing the efficiency of the suggested approach under complicated environmental and parametric conditions.

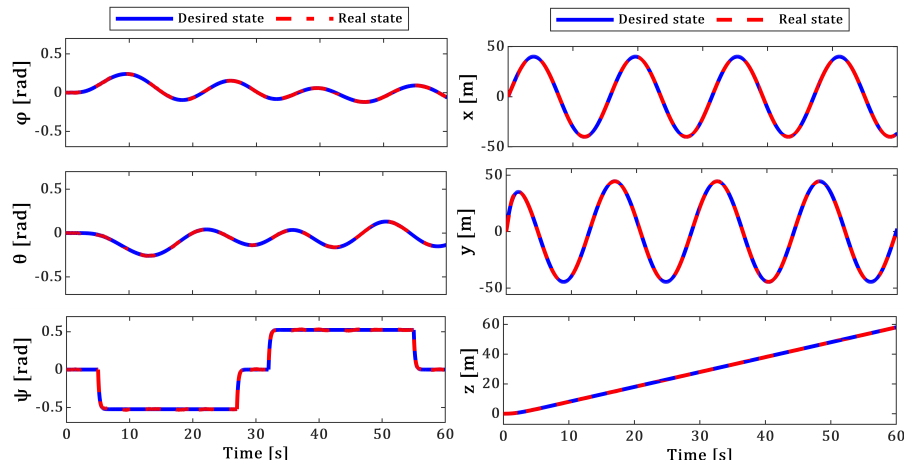


Figure 4: Attitude and position tracking in the presence of uncertainties and wind disturbances.

### Condition 2: Trajectory tracking in the presence of wind disturbances, uncertainties, and actuator faults

The actuator fault profile is resumed in table 2. Where  $W(t) = \sum_{k=0}^5 0.4^k \cos(3^k \pi t)$  is the Weierstrass function-type fault that is smooth but non-differentiable.

Table 2: Actuator faults  $f_{a1}$  and  $f_{a4}$  profile

$f_{a1}(\phi)$	$f_{a4}(z)$	Occurrence time	Fault type
0	0	$0 \leq t < 10$ s	Fault free
5	5	$10 \leq t < 20$ s	Bias fault
$-0.4U_2(t)$	$-0.3U_1(t)$	$20 \leq t < 30$ s	Loss of effectiveness fault
$-U_2(t) + 5$	$-U_1(t) + 5$	$30 \leq t < 40$ s	Actuator Stuck
$-U_2(t) - 5$	$-U_1(t) - 5$	$40 \leq t < 50$ s	Actuator Stuck
$2W(t)$	$1W(t)$	$50 \leq t < 60$ s	Weierstrass function

Gaussian noise is applied to the actuator faults to test the robustness of the system. Specifically, a Gaussian noise  $\mathcal{N}_{a1}(0.05, 0.05^2)$  is added to  $f_{a1}$ , and  $\mathcal{N}_{a4}(0.005, 0.005^2)$  is introduced to  $f_{a4}$ .

The corresponding FE of  $f_{a1}$  and  $f_{a4}$  in each actuator is shown in Figure 5. It demonstrates good FE accuracy with RMSE (Root Mean Square Error) for  $f_{a1}$  and  $f_{a4}$  hovering around  $10^{-14}$ .

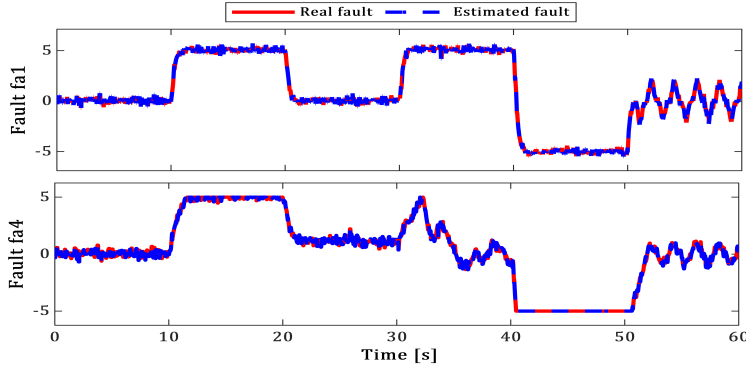


Figure 5: Actuator fault estimation.

### Condition 3: Trajectory tracking in the presence of wind disturbances, uncertainties, actuator and sensor faults

In addition to the actuator faults previously tested, sensor faults detailed in Table 3 were introduced. Furthermore, Gaussian noise  $N(0.01, 0.01^2)$  is added to  $f_{s4}$  and  $f_{s5}$ .

Table 3: Sensor faults  $f_{s1}(\phi)$ ,  $f_{s4}(x)$ ,  $f_{s5}(y)$  profile

$f_{s1}(\phi)$	$f_{s4}(x)$	$f_{s5}(y)$	Occurrence time	Fault type
0	0	0	$0 \leq t < 10$ s	Fault free
1	5	5	$10 \leq t < 20$ s	Bias fault
$0.1t$	$0.6t$	$0.6t$	$20 \leq t < 30$ s	Drift fault
$-0.6\dot{\phi}(t)$	$-0.25\dot{x}(t)$	$-0.25\dot{y}(t)$	$30 \leq t < 40$ s	Loss of effectiveness fault
$-\dot{\phi}(t) + 1$	$-\dot{x}(t) + 5$	$-\dot{y}(t) + 5$	$40 \leq t < 50$ s	Stuck Sensor fault
$0.4W(t)$	$4W(t)$	$4W(t)$	$50 \leq t < 60$ s	Weierstrass function fault

Sensor fault estimation of  $f_{s1}$ ,  $f_{s4}$ , and  $f_{s5}$  is shown in Figure 6. It illustrates the precise estimation of sensor faults. The results highlight the robustness of the capability of the developed NUIO to accurately estimate these faults without being significantly impacted by these disturbances, with RMSE for  $f_{s1}$ ,  $f_{s4}$ , and  $f_{s5}$  remaining close to zero.

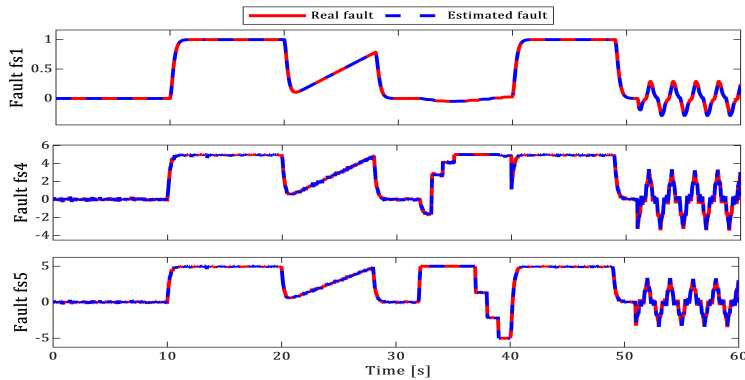


Figure 6: Sensor FE of  $f_{s1}$ ,  $f_{s4}$ , and  $f_{s5}$

Figure 7 illustrates the system's tracking performance in the presence of actuator and sensor faults. Despite the presence of some fluctuations in the states, particularly in  $\phi$ ,  $x$ , and  $y$ , the tracking remains robust, showcasing the effectiveness of the proposed FTC strategy.

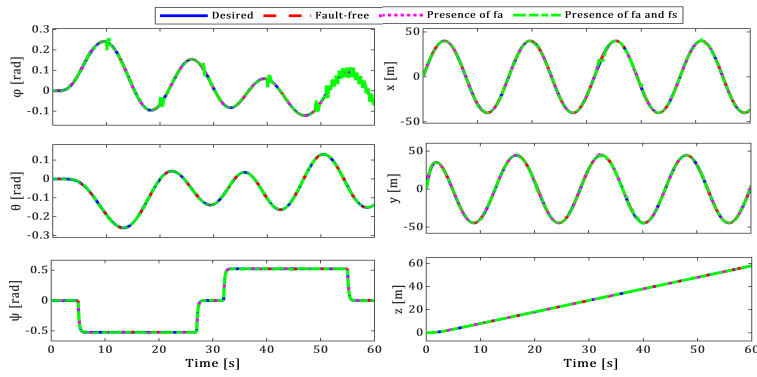


Figure 7: Trajectories along attitude and position in the presence of actuator and sensor faults

The global trajectory of the quadrotor in 3D along the ( $X$ ,  $Y$ ,  $Z$ ) axis, as depicted in Figure 8, demonstrates a stable and accurate flight path despite the presence of actuator and sensor faults.

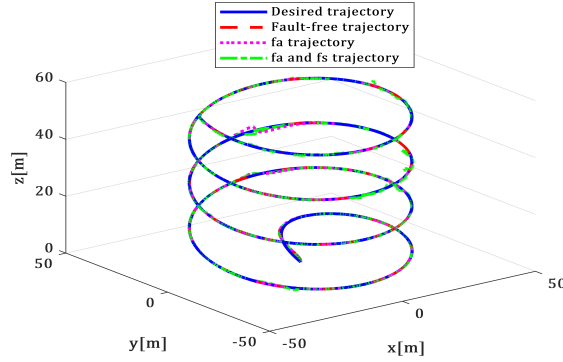


Figure 8: Global trajectory of the quadrotor in 3D in presence of actuators and sensor faults.

The plots in Figure 9 show that the tracking errors for  $\theta$ ,  $\psi$ , and  $z$  remain small under all conditions. In contrast, the errors for  $\phi$ ,  $x$ , and  $y$  exhibit noticeable increases when both actuator and sensor faults are present. Despite that, the attitude mean error stays below  $10^{-5}$  rad, and the position mean error remains under  $10^{-3}$  m.

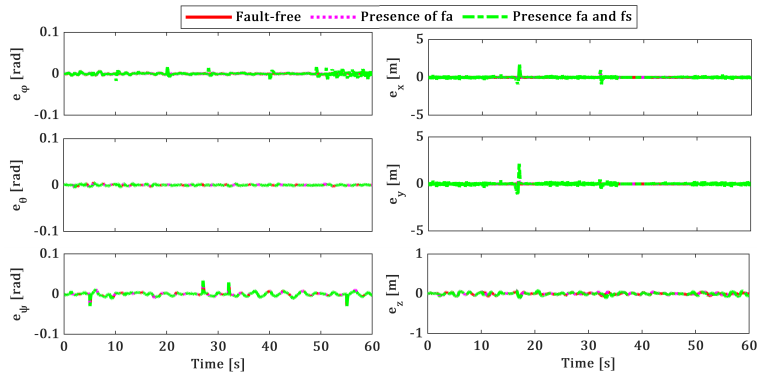


Figure 9: Tracking errors in the presence of actuator and sensor faults.

The control inputs  $U_1$ ,  $U_2$ ,  $U_3$ , and  $U_4$  of the system, as shown in Figure 10, demonstrate the effectiveness of the proposed FTC approach in the presence of actuator and sensor faults. The generated control signals are both physically realizable and robust, highlighting the practicality of the strategy. Furthermore, small control inputs ensure low energy consumption is maintained.

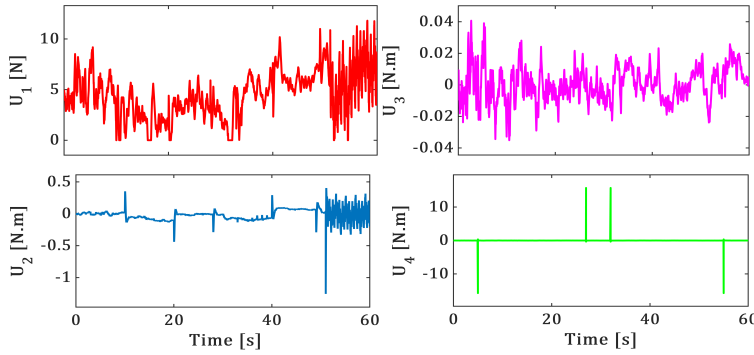


Figure 10: Control inputs of actuators in presence of actuator and sensor faults.

The Table 4 comparing the RMSE for the three different conditions provides valuable insights into the quadrotor's performance.

Table 4: RMSE values for attitude (on  $\text{rad}$ ) and position (on  $\text{m}$ ) in different scenarios.

Condition	RMSE ( $\phi$ )	RMSE ( $\theta$ )	RMSE ( $\psi$ )	RMSE ( $x$ )	RMSE ( $y$ )	RMSE ( $z$ )
<b>Condition 1</b>	$1.38 \times 10^{-3}$	$1.45 \times 10^{-3}$	$4.66 \times 10^{-3}$	$1.22 \times 10^{-3}$	$1.24 \times 10^{-3}$	$2.44 \times 10^{-2}$
<b>Condition 2</b>	$1.38 \times 10^{-3}$	$1.45 \times 10^{-3}$	$4.66 \times 10^{-3}$	$2.80 \times 10^{-2}$	$2.75 \times 10^{-2}$	$2.66 \times 10^{-2}$
<b>Condition 3</b>	$3.38 \times 10^{-3}$	$1.45 \times 10^{-3}$	$4.66 \times 10^{-3}$	0.15	0.16	$2.80 \times 10^{-2}$

Under the first condition, where the system faces only external disturbances and uncertainties, there is minimal deviation in the RMSE for both attitude and position. In the second condition, with the introduction of actuator faults, the RMSE values show little change, demonstrating the robustness of the control strategy. In the third condition, which includes both actuator and sensor faults, the attitude RMSE values closely resemble those from the previous condition. However, there is an increase in the RMSE for the  $x$  and  $y$  coordinates, while the  $z$  coordinate RMSE continues to mirror the second condition's values.

## 6 Conclusion

This study begins with a short description of the quadrotor's nonlinear dynamic model, which takes into consideration the nonlinearities and high-order nonholonomic constraints of the system. In the presence of uncertainties and external disturbances, a novel NUIO is proposed to estimate actuator and sensor faults simultaneously, without requiring certain system matrices to have a specific rank to ensure that faults or disturbances can be isolated without ambiguity; the FE unit design problem is formulated as an observer-based robust control problem, and it is solved using  $\mathcal{H}_\infty$  optimization in an LMI formulation. An adaptive backstepping sliding mode FTC controller using the NUIO-based FE is constructed.

To evaluate the performance of the proposed controller, we executed simulations in MATLAB across three conditions. The results of the simulation clearly illustrate the good performance of the adopted strategy, as it made it possible to precisely estimate the faults and to ensure stability and trajectory tracking. The highest RMSE for attitude in the presence of actuator faults is lower than  $10^{-3}$  rad, and the highest RMSE for position is lower than  $10^{-2}$  m. Additionally, in conditions involving both actuator and sensor faults, the highest RMSE for attitude remains below  $10^{-3}$  rad, while for position, it is lower than 0.2 m. The proposed FTC techniques demonstrate robust performance in mitigating the effects of wind disturbances and uncertainties, maintaining acceptable tracking accuracy in various scenarios, and addressing different environmental challenges effectively.

Future research directions will extend this study to real-world implementation and extreme operational conditions, including scenarios with severe environmental disturbances and rapid multiple fault

occurrences. Additionally, experimental validation through hardware implementation will be conducted to evaluate the method's performance under realistic operating conditions with actual sensor noise and hardware constraints.

## References

- [1] Baldini, A., Felicetti, R., Freddi, A., Monteriù, A., "Fault-Tolerant Control of a Variable-Pitch Quadrotor under Actuator Loss of Effectiveness and Wind Perturbations," *Sensors and Transducers*, vol. 23, no. 10, p. 4907, May 2013.
- [2] Nguyen, N., Hong, S., "Fault-Tolerant Control of Quadcopter UAVs Using Robust Adaptive Sliding Mode Approach," *Energies*, vol. 12, p. 95, December 2018.
- [3] Nguyen, N., Hong, S., "Active Fault-Tolerant Control of a Quadcopter against Time-Varying Actuator Faults and Saturation Using Sliding Mode Backstepping Approach," *Applied Sciences*, vol. 9, p. 4010, September 2019.
- [4] Wang, B., Yu, X., Mu, L., Zhang, Y., "Disturbance observer-based adaptive fault-tolerant control for a quadrotor helicopter subject to parametric uncertainties and external disturbances," *Mechanical Systems and Signal Processing*, vol. 120, pp. 727-743, April 2019.
- [5] Ma, H., Liu, Y., Li, T., Yang, G.-H., "Nonlinear High-Gain Observer-Based Diagnosis and Compensation for Actuator and Sensor Faults in a Quadrotor Unmanned Aerial Vehicle," *IEEE Transactions on Industrial Informatics*, vol. 15, no. 1, pp. 550-562, August 2019.
- [6] Nguyen, N.-P., Pitakwatchara, P., "Attitude Fault-Tolerant Control of Aerial Robots with Sensor Faults and Disturbances," *Drones*, vol. 7, p. 156, February 2023.
- [7] Ezzara, A., Ouadine, A. Y., Ayad, H., "Adaptive Observer-based Fault-Tolerant Control for Actuator Faults in Quadrotor UAV," in *2024 International Conference on Global Aeronautical Engineering and Satellite Technology (GAST)*, pp. 1-5, 2024.
- [8] Ouadine, A. Y., Mjahed, M., Ayad, H., El Kari, A., "UAV Quadrotor Fault Detection and Isolation Using Artificial Neural Network and Hammerstein-Wiener Model," *Studies in Informatics and Control*, vol. 29, no. 3, pp. 317-328, 2020.
- [9] Zou, P., Hou, B., Jiang, L., Zhang, Z., "Bearing Fault Diagnosis Method Based on EEMD and LSTM," *International Journal of Computers Communications and Control*, vol. 15, no. 1, 2020.
- [10] Moldovan, O., Ghincu, R., Moldovan, A., Noje, D., Tarca, R., "Fault Detection in Three-phase Induction Motor based on Data Acquisition and ANN based Data Processing," *International Journal of Computers Communications and Control*, vol. 17, no. 3, 2022.
- [11] Gao, Z., Liu, X., Chen, M., "Unknown Input Observer Based Robust Fault Estimation for Systems Corrupted by Partially-Decoupled Disturbances," *IEEE Transactions on Industrial Electronics*, vol. 63, pp. 1-1, January 2015.
- [12] Chen, J., Patton, R., Zhang, H.-Y., "Design of unknown input observers and robust fault detection filters," *International Journal of Control*, vol. 63, pp. 85-105, February 2007.
- [13] Chen, W., Saif, M., "Unknown input observer design for a class of nonlinear systems: An LMI approach," in *Proceedings of the American Control Conference*, vol. 2006, pp. 5 pp.-, July 2006.
- [14] Xia, J., Jiang, B., Zhang, K., "UIO-Based Practical Fixed-Time Fault Estimation Observer Design of Nonlinear Systems," *Symmetry*, vol. 14, p. 1618, August 2022.
- [15] Hashemi, M., Egoli, A., Naraghi, M., Tan, C., "Saturated Fault Tolerant Control Based on Partially Decoupled Unknown-Input Observer: A New Integrated Design Strategy," *IET Control Theory and Applications*, July 2019.

- [16] Lan, J., Patton, R. J., "Integrated fault estimation and fault-tolerant control for uncertain Lipschitz non-linear systems," *International Journal of Robust and Nonlinear Control*, vol. 27, no. 5, pp. 761-780, 2016.
- [17] Bouadi, H., Tadjine, M., Bouchoucha, M., "Modelling and stabilizing control laws design based on backstepping for an UAV type-quadrotor," *IFAC Proceedings Volumes*, vol. 40, no. 15, pp. 245-250, 2007.
- [18] Li, F., Song, W.-P., Song, B., Jiao, J., "Dynamic Simulation and Conceptual Layout Study on a Quad-Plane in VTOL Mode in Wind Disturbance Environment," *International Journal of Aerospace Engineering*, vol. 2022, pp. 1-24, January 2022.
- [19] Li, F., Song, W.-P., Song, B., Zhang, H., "Dynamic modeling, simulation, and parameter study of electric quadrotor system of Quad-Plane UAV in wind disturbance environment," *International Journal of Micro Air Vehicles*, vol. 13, January 2021.
- [20] Cole, K., "Reactive trajectory generation and formation control for groups of UAVs in windy environments," Washington, 2018.
- [21] Boskovic, J., Mehra, R., "Stable adaptive multiple model-based control design for accommodation of sensor failures," in *Proceedings of the American Control Conference*, vol. 3, pp. 2046 - 2051, February 2002.
- [22] Jinghui, P., Lili, Q., Kaixiang, P., "Sensor and Actuator Fault Diagnosis for Robot Joint Based on Deep CNN," *Entropy*, vol. 23, p. 751, June 2021.
- [23] Balaban, E., Saxena, A., Bansal, P., Goebel, K. F., Curran, S., "Modeling, Detection, and Disambiguation of Sensor Faults for Aerospace Applications," *IEEE Sensors Journal*, vol. 9, no. 12, pp. 1907-1917, 2009.
- [24] Silva, J., Saxena, A., Balaban, E., Goebel, K., "A knowledge-based system approach for sensor fault modeling, detection and mitigation," *Expert Systems with Applications*, vol. 39, pp. 10977-10989, September 2012.
- [25] Derafa, L., Madani, T., Benallegue, A., "Dynamic modelling and experimental identification of four rotor helicopter parameters," in *2006 IEEE International Conference on Industrial Technology*, pp. 1834-1839, 2006.



Copyright ©2024 by the authors. Licensee Agora University, Oradea, Romania.

This is an open access article distributed under the terms and conditions of the Creative Commons Attribution-NonCommercial 4.0 International License.

Journal's webpage: <http://univagora.ro/jour/index.php/ijccc/>



This journal is a member of, and subscribes to the principles of,  
the Committee on Publication Ethics (COPE).

<https://publicationethics.org/members/international-journal-computers-communications-and-control>

*Cite this paper as:*

Ezzara, A.; Ouadine, A.Y.;Ayad, H. (2024). Adaptive-Backstepping-Sliding-Mode Fault-Tolerant Control of Quadrotor UAV in presence of external disturbances, uncertainties, and Simultaneous Actuator and Sensor faults,*International Journal of Computers Communications & Control*, 19(1), 4xyz, 2024.

<https://doi.org/10.15837/ijccc.2024.1.4xyz>